Acta Geochim (2017) 36(2):276–290
DOI 10.1007/s11631-017-0145-7

ORIGINAL ARTICLE

Carboniferous Alaskan-type complex along the Sino–Mongolian boundary, southern margin of the Central Asian Orogenic Belt

Yuruo Shi[1] · Linlin Li[1] · Alfred Kröner[1,2] · Jing Ding[1] · Wei Zhang[1] · Zengbao Huang[3] · Ping Jian[1]

Received: 8 December 2016 / Revised: 16 January 2017 / Accepted: 6 February 2017 / Published online: 17 February 2017

Abstract We present zircon ages and geochemical data for the Hongshishan Carboniferous Alaskan-type mafic–ultramafic complex exposed in the Beishan area along the Sino–Mongolian boundary, southern margin of the Central Asian Orogenic Belt. This complex mainly consists of dunite, harzburgite, lherzolite, wehrlite, and gabbro, which intrudes Early Carboniferous volcanic rocks and reveals a zoned structure. Zircons of a gabbro sample yielded a $^{206}Pb/^{238}U$ age of 357 ± 4 Ma, reflecting the time of Early Carboniferous magmatism. Zircon ages were also obtained for an andesite (322 ± 3 Ma) and a basaltic andesite (304 ± 2 Ma). High *initial* Nd isotope whole-rock values suggest that the Hongshishan gabbro [$\varepsilon_{Nd(t)} = +9.6 - +10.2$] and basalt [$\varepsilon_{Nd(t)} = +10.0 - +10.8$] were derived from a depleted mantle source. Slightly lower $\varepsilon_{Nd(t)}$ values for the ultramafic rocks [$\varepsilon_{Nd(t)} = +8.5 - +8.7$] suggest some interaction of the parental magma with the continental crust. In contrast, the Late Carboniferous Quershan samples in this area represent subduction-related arc volcanic rocks with Adakite-like compositions. The early Carboniferous Hongshishan Alaskan-type complex was interpreted to represent the remnants of a magma chamber that crystallized at the base of a mature island arc, whereas the Quershan island arc volcanic rocks suggest the resurrection of the subduction process after arc-continent collision and uplift of the roots of the arc.

Keywords Alaskan-type complex · Carboniferous · Zircon age · Sino–Mongolian boundary · CAOB

✉ Yuruo Shi
shiyuruo@bjshrimp.cn

[1] Beijing SHRIMP Center, Institute of Geology, Chinese Academy of Geological Sciences, Beijing 100037, China

[2] Institut für Geowissenschaften, Universität Mainz, 55099 Mainz, Germany

[3] Geological Survey of Gansu Province, Lanzhou 735000, China

1 Introduction

Alaskan-type complexes have been well documented in the geological literature (e.g., Taylor 1967; Murray 1972; Irvine 1974; Himmelberg and Loney 1994; Fershtater et al. 1997; Helmy and El Mahallawi 2003). These complexes range in size from sills only a few meters wide to intrusions that are approximately 10 km in maximum exposed dimension (Himmelberg and Loney 1994). They are markedly concentrically zoned and, in most cases, are roughly circular or elliptical in shape, and/or pipe-like in cross-section. These complexes are generally composed of dunite, wehrlite, olivine clinopyroxenite, clinopyroxenite, hornblende clinopyroxenite, and gabbro, but the complete sequence of lithologies is rarely observed (Himmelberg and Loney 1994).

The Central Asian Orogenic Belt (CAOB, Fig. 1A) is a giant accretionary orogen (Windley et al. 2007) and is bounded by the Siberian, Tarim, and North China cratons (Jahn et al. 2000; Badarch et al. 2002). The CAOB records a complex evolution from the latest Mesoproterozoic to Late Paleozoic (Tang 1990; Dobretsov et al. 1995; Xiao et al. 2003; Jian et al. 2007, 2008; Kröner et al. 2014). It is likely that this large, long-lived orogenic domain evolved through the operation of several subduction systems with different polarities, through the closure of multiple ocean basins, and through the collision/accretion of arcs and

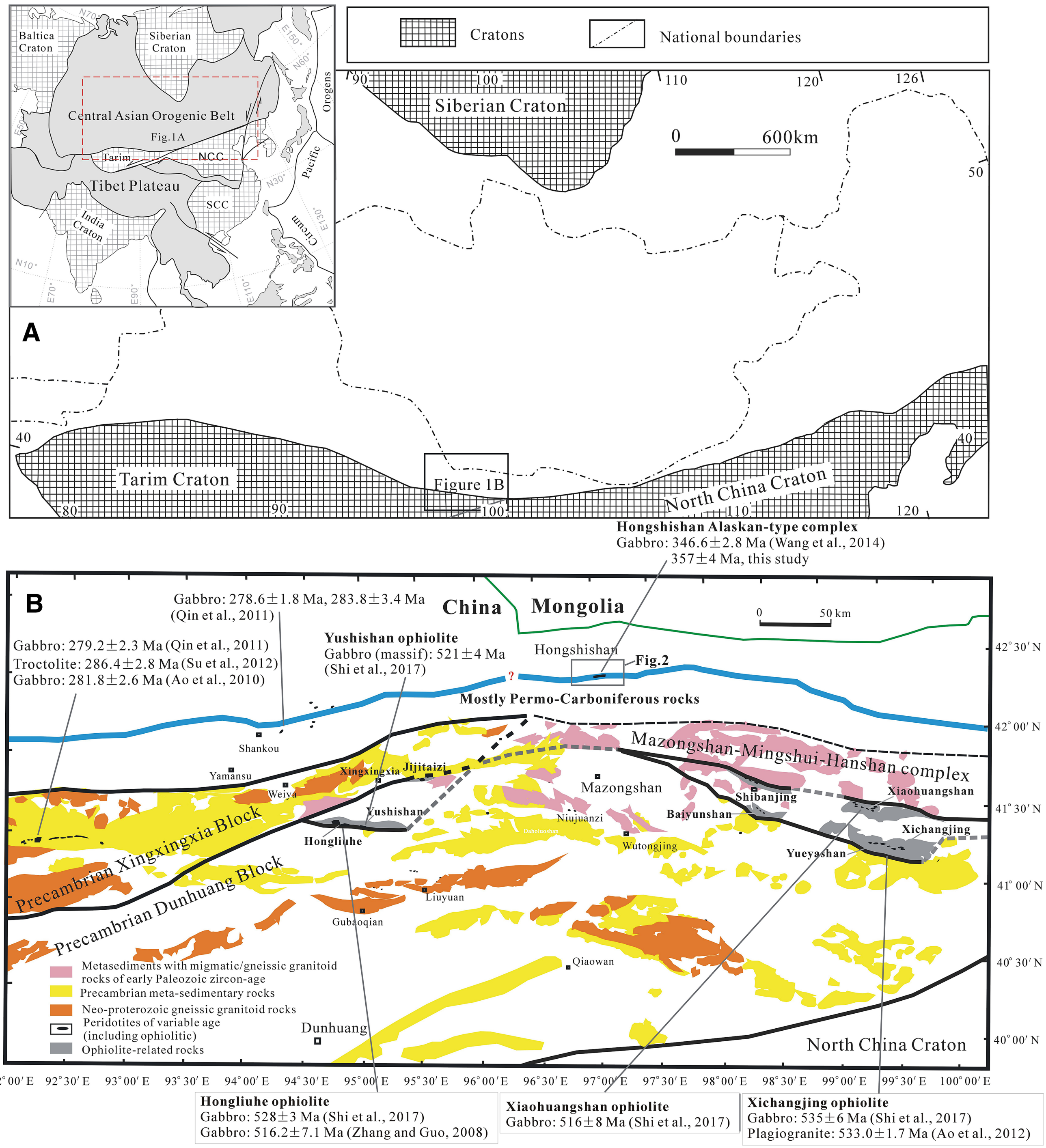

Fig. 1 Geological sketch map of the southeastern CAOB (the *inset* map of **a** compiled after Jahn et al. 2000). Position of Fig. 2 is marked

microcontinents (Coleman 1989; Mossakovskii et al. 1993; Kröner et al. 2007, 2014; Windley et al. 2007).

Mafic–ultramafic complexes, most of which were identified as ophiolites or post-orogenic intrusions, are widely distributed along the southern margin of the CAOB (Jian et al. 2010a, b, 2012; Xiao et al. 2010; Qin et al. 2011; Su et al. 2011, 2012). Here we present SHRIMP zircon U–Pb ages and geochemical data for a Carboniferous Alaskan-type mafic–ultramafic complex and associated volcanic rocks in the Hongshishan area, Gansu Province, China, and we discuss their petrogenesis as part of the evolution of the CAOB.

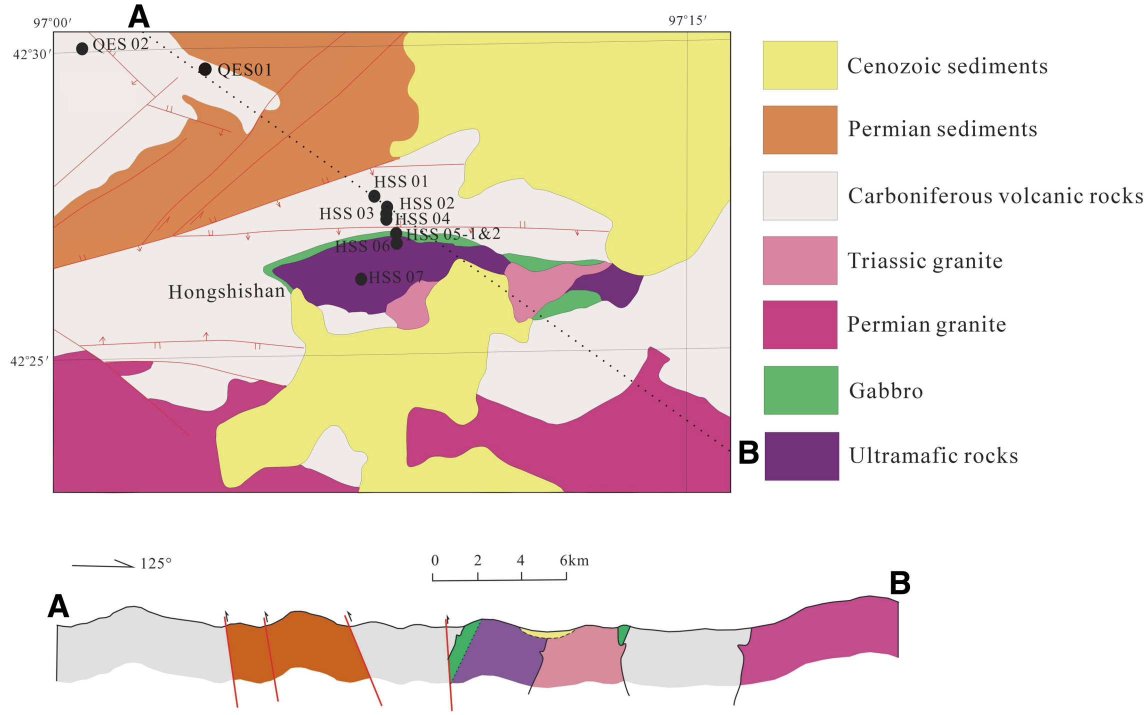

Fig. 2 Simplified geological map of Hongshishan area, Gansu Province, China. The locations of samples are indicated

2 Geological setting and field relations

The Hongshishan area, Gansu Province, is situated along the Sino–Mongolian boundary (Fig. 1B), and belongs to the southern margin of the CAOB. The Hongshishan mafic–ultramafic complex mainly consists of dunite, harzburgite, lherzolite, wehrlite, and gabbro, and shows a zoned structure (Fig. 2). The exposure of ultramafic rocks is 5 km long and up to 3 km wide with an exposed area of ca. 14 km^2; gabbro is found discontinuously along the margin of the ultramafic rocks, which intrudes Early Carboniferous volcanic rocks (basalts and andesites). These rocks occur along the Hongshishan suture zone, which includes Devonian, Carboniferous, and Permian volcanic rocks.

Harzburgite and dunite are exposed on the southern margin of the mafic–ultramafic complex whereas wehrlite, harzburgite, lherzolite, and dunite, with the occurrence of chromite, are exposed in the central part. Wehrlite and dunite are only found on the northern margin of the complex. Most ultramafic rocks are medium-to coarse-grained adcumulates (Wei et al. 2004). Textures are generally subhedral to anhedral granular with mutually interfering, gently curved grain boundary segments. Chromian spinel is an accessory mineral in dunite (Huang and Jin 2006).

Harzburgite, lherzolite, gabbro, basalt, and andesite samples were collected for geochemical studies, and from these samples, one gabbro (N42°27′15″; E97°08′07″), one andesite (N42°29′54″; E97°04′21″), and one basaltic andesite sample were chosen for SHRIMP zircon U–Pb dating.

3 Analytical methods

Samples were crushed, contamination-free, to less than 200 mesh. Major and trace elements were analyzed by both XRF (X-ray fluorescence spectrometry) and ICP-MS (Inductively coupled plasma mass spectrometry) at the National Research Center for Geoanalysis, Chinese Academy of Geological Sciences, Beijing. The precision for major elements was about 1%, and for trace element analyses it was generally better than 10%. The analytical results are listed in Table 1.

Zircons were extracted from ca. 20 kg of fresh rock. The crushed sample was panned and then underwent electromagnetic isodynamic heavy mineral separation. Approximately 100 grains of each sample were then handpicked using a binocular microscope. These were mounted onto an epoxy resin disc together with several grains of the standard zircon TEMORA (Black et al. 2003). Then, these were both ground down and polished so that their interiors were exposed. Zircons were then photographed by optical microscopy, and cathodoluminescence (CL) images were obtained using a HITACHI S-3000N SEM with accelerating voltage of 10 kV and an electron current of 100 μA.

Table 1 Major oxides, REE and trace element composition of samples

Locality/unit	Hongshishan								Quershan	
Sample no.	HSS06	HSS07	HSS05-1	HSS05-2	HSS02	HSS03	HSS04	HSS01	QES01	QES02
Lithology	Harzburgite	Lherzolite	Gabbro	Leucogabbro	Basalt	Basalt	Basalt	Basaltic andesite	Andesite	Basaltic andesite
Note			357 ± 4 Ma		N-MORB-like, with arc signature				322 ± 3 Ma	304 ± 2 Ma
Oxide (%)										
SiO_2	40.55	36.80	49.71	46.79	46.87	47.3	43.4	52.71	60.7	50.02
TiO_2	0.06	0.04	0.33	0.07	1.46	1	1.01	0.91	0.77	1.26
Al_2O_3	1.38	1.75	16.8	29.24	13.39	13.61	11.99	15.44	15.54	19.8
Fe_2O_3	6.01	6.42	2.09	0.86	5.4	5.36	2.83	3.29	2.69	3.24
FeO	1.94	2.86	4.13	0.54	7.13	8.08	9.23	4.92	3.57	5.42
MnO	0.13	0.12	0.12	0.04	0.21	0.2	0.19	0.14	0.12	0.15
MgO	34.82	34	8	0.74	7.5	7.97	6.89	7.85	3.18	3.54
CaO	3.37	3.53	14.11	15.45	10.82	10.65	10.05	7.03	4.12	5.89
Na_2O	0.03	0.08	1.83	3.09	1.96	1.66	1.83	3.36	4.42	4.21
K_2O	0.01	0.01	0.03	0.53	0.05	0.04	0.01	0.93	1.86	1.87
P_2O_5	0.01	0.01	0.01	0	0.11	0.03	0.01	0.14	0.19	0.31
H_2O	9.98	10.34	1.86	1.92	3.44	2.92	5.48	2.44	1.88	4.12
CO_2	0.45	4	0.31	0.21	1	0.5	7.19	0.45	0.52	0.29
Total	98.74	99.96	99.33	99.48	99.34	99.32	100.11	99.61	99.56	100.12
REE and trace elements (*ppm*)										
La	0.18	0.07	0.36	0.32	4.16	0.69	0.5	9.34	14.7	10.7
Ce	0.45	0.2	1.13	0.81	11.7	2.31	1.7	21.5	32.3	24.8
Pr	0.06	<0.05	0.28	0.12	2.23	0.55	0.42	3.12	4.82	4.02
Nd	0.31	0.16	1.92	0.65	12.3	3.81	2.85	14.2	19.8	18.6
Sm	0.1	<0.05	1.01	0.2	4.28	1.79	1.67	3.73	4.46	4.66
Eu	<0.05	<0.05	0.45	0.3	1.45	0.8	1.11	1.15	1.08	1.56
Gd	0.19	0.09	1.59	0.2	5.85	2.88	3.02	3.85	4.12	4.55
Tb	<0.05	<0.05	0.35	<0.05	1.06	0.59	0.58	0.64	0.58	0.63
Dy	0.23	0.1	2.45	0.21	7.22	4.24	4.26	3.92	3.56	3.77
Ho	0.05	<0.05	0.57	0.05	1.56	1	0.95	0.82	0.69	0.75
Er	0.2	0.07	1.83	0.15	4.76	3.23	3.04	2.49	2.14	2.19
Tm	<0.05	<0.05	0.24	<0.05	0.64	0.46	0.42	0.34	0.28	0.27
Yb	0.16	0.08	1.75	0.15	4.41	3.16	3.07	2.31	2.14	2.02
Lu	<0.05	<0.05	0.25	<0.05	0.66	0.49	0.45	0.36	0.32	0.3
Y	1.25	0.58	13.5	1.26	34.8	23.7	22.7	19.4	17.7	16.7
Sc	24.7	9.26	62.8	2.52	55.4	54.3	52.7	33.5	19.5	25.2
V	78.8	35.7	279	16	450	414	421	233	148	292
Cr	8581	4516	338	19.4	256	266	181	376	43.4	12.9
Co	108	138	33.8	5.89	37.6	55.4	50.3	43.6	15.3	24.8
Ni	1604	1981	132	19.7	93.7	115	84.2	168	19.3	12.9
Cu	3.55	25.5	136	7.71	90.2	50	51.7	26.6	15.5	73.4
Zn	42.3	39.7	33.4	7.47	97.8	81.8	101	72.3	76.8	84.1
Ga	2.13	2.1	13.6	16.2	17.2	15.9	14.5	15.8	17.5	19.4
Rb	0.39	0.42	0.55	10.3	1.4	0.32	0.61	18.5	36.5	45.3
Sr	11.7	43.1	61.6	72.9	141	81.6	63.9	281	478	629
Zr	1.97	0.77	7.47	2.09	74.6	21.3	14.3	89.5	148	71.3
Nb	0.06	<0.05	0.06	0.1	2.68	0.27	0.11	2.89	3.4	2.49

Table 1 continued

Locality/unit	Hongshishan								Quershan	
Sample no.	HSS06	HSS07	HSS05-1	HSS05-2	HSS02	HSS03	HSS04	HSS01	QES01	QES02
Lithology	Harzburgite	Lherzolite	Gabbro	Leucogabbro	Basalt	Basalt	Basalt	Basaltic andesite	Andesite	Basaltic andesite
Note			357 ± 4 Ma		N-MORB-like, with arc signature				322 ± 3 Ma	304 ± 2 Ma
Cs	<0.05	0.05	0.08	0.32	0.11	0.12	0.14	1.62	0.85	1.89
Ba	5.01	5.24	7.26	111	12.4	10.8	17.4	220	503	345
Hf	0.06	<0.05	0.41	0.07	2.66	1.00	0.79	2.67	4.73	2.44
Pb	0.36	0.56	0.49	0.71	3.05	0.96	0.48	2.42	6.39	2.23
Th	<0.05	<0.05	<0.05	<0.05	0.41	0.05	0.05	1.85	3.62	0.87
U	0.34	0.38	0.28	0.12	0.17	0.13	0.28	0.65	1.10	0.42

U–Th–Pb analyses were performed in several analytical sessions using a SHRIMP II instrument at the Beijing SHRIMP Center, Institute of Geology, Chinese Academy of Geological Sciences. Analytical procedures followed those of Williams (1998). Magmatic ages reported in the text have a weighted mean $^{206}Pb/^{238}U$ ages, and the uncertainties are cited at the 95% confidence limit. Chi square (χ^2) was employed to test whether an age population met the statistical requirements. When $\chi^2 = 1$, the error of the weighted mean age was consistent with the error of individual analyses, and there was no excess scatter (Black and Jagodzinski 2003). The analytical results are listed in Table 2.

Sr–Nd whole-rock isotopic analyses were conducted in the Isotope Laboratory, Institute of Geology, Chinese Academy of Geological Sciences, Beijing, following procedures described in Zhang et al. (1994), and the results are listed in Table 3.

4 Results

4.1 Major and trace elements

The volcanic rocks from Hongshishan are basalt and basaltic andesite in composition (Table 1) with low to medium potassic (0.01%–0.93%) and high TiO_2 contents (0.91%–1.46%). Two samples (HSS03, HSS04) exhibit N-MORB-like, LREE-depleted REE patterns (Fig. 3), and lower total REE contents than N-MORB, which is consistent with island arc tholeiites (IATs) (e.g., Hawkins 2003). The other two basalts (HSS01, HSS02) display flat REE patterns (Figs. 3, 4). The REE compositional diversity of these volcanic rocks signifies different mantle sources. A TiO_2 versus V plot (Fig. 5; Shervais 1982), a Th/Yb versus Nb/Yb plot (Fig. 5; Pearce 2008) and a MORB-normalized multi-element variation diagram indicate an IAT affinity for these samples and are diagnostic SSZ signatures, most likely produced in response to aqueous fluids/melts expelled from a subducting slab (Shervais 2001).

However, the volcanic rocks from Quershan are basaltic andesite and andesite and have intermediate to high silica (50.02 wt%–60.70 wt%), high Al_2O_3 (15.54%–19.80%), higher Na_2O than K_2O ($Na_2O > K_2O$, $Na_2O/K_2O = 2.38$–2.51), with medium-potassic (1.86%–1.87%). LREE-enriched REE patterns, LILEs (large-ion lithophile elements) enrichment over HFSEs (high field-strength elements), coupled with a pronounced negative Nb anomaly relative to Th, U and La (Fig. 4) indicate the volcanic rocks are similar to those island arc volcanic rocks (Gill 1981).

Gabbro sample HSS05-1 exhibits a LREE-depleted, N-MORB-like REE pattern, and has a SSZ signature, i.e. LILE enrichment over HFSE and a pronounced Nb depletion (Fig. 4). Leucogabbro sample HSS05-2 has positive Eu, and Sr anomalies that indicate accumulation of plagioclase (Fig. 4). The ultramafic rocks (HSS06, HSS07) also display flat REE patterns (Fig. 3).

4.2 Zircon ages

Zircons from gabbro sample HSS05-1 are euhedral, and their cathodoluminescence (CL) images (Fig. 6A) show broad and rhythmically zoned oscillatory patterns characteristic of magmatic crystallization. Sixteen grain analyses form a concordant group in the concordia diagram with a weighted mean age of 357 ± 4 Ma ($\chi^2 = 1.53$) (Table 2; Fig. 7A) that we have interpreted to reflect the time of gabbro emplacement.

Andesite sample QES01 contains euhedral, prismatic crystals that display oscillatory zoning under CL (Fig. 6B), indicating a magmatic origin. Ten analyses yielded a weighted mean $^{206}Pb/^{238}U$ age of 322 ± 3 Ma ($\chi^2 = 0.83$) (Table 2; Fig. 7B) that we have interpreted to reflect the

Table 2 SHRIMP U–Pb analytical data for zircons of this study

Spot	U (ppm)	Th (ppm)	Th/U	Pb* (ppm)	$^{206}Pb_c$ (%)	$^{206}Pb^*/^{238}U$	error 1 σ	$^{207}Pb^*/^{235}U$	error 1 σ	$^{207}Pb^*/^{206}Pb^*$	error 1 σ	Age (Ma) $^{206}Pb^*/^{238}U$	error 1 σ	Age (Ma) $^{207}Pb^*/^{235}U$	error 1 σ	Age (Ma) $^{207}Pb^*/^{206}Pb^*$	error 1 σ
HSS05-1 Gabbro																	
1.1	99	36	0.37	5	0.02	0.0555	0.0023	0.376	0.044	0.0491	0.0051	348	14	324	33	152	225
2.1	43	31	0.71	3	0.06	0.0539	0.0029	0.246	0.082	0.0331	0.0106	339	18	223	69	–	–
3.1	17	10	0.56	1	0.16	0.0554	0.0052	0.223	0.339	0.0292	0.0440	348	32	204	249	–	–
4.1	48	10	0.21	3	0.03	0.0579	0.0018	0.437	0.057	0.0547	0.0067	363	11	368	41	400	303
5.1	67	13	0.20	4	0.02	0.0600	0.0023	0.463	0.066	0.0560	0.0075	376	14	386	47	451	327
6.1	38	9	0.24	2	0.05	0.0540	0.0031	0.372	0.107	0.0500	0.0138	339	19	321	83	196	808
7.1	25	7	0.28	1	0.06	0.0549	0.0026	0.368	0.089	0.0487	0.0113	344	16	318	68	131	659
8.1	8	3	0.42	0	0.18	0.0568	0.0063	0.770	0.209	0.0982	0.0230	356	39	579	127	1591	515
9.1	14	7	0.52	1	0.14	0.0537	0.0040	0.257	0.123	0.0348	0.0161	337	25	233	104	–	–
10.1	11	4	0.38	1	0.15	0.0594	0.0040	0.341	0.288	0.0416	0.0347	372	24	298	246	–	–
11.1	92	33	0.36	5	0.02	0.0565	0.0017	0.417	0.039	0.0535	0.0045	354	11	354	28	351	203
12.1	125	54	0.43	8	0.01	0.0590	0.0021	0.464	0.062	0.0570	0.0071	369	13	387	44	493	299
13.1	59	15	0.26	3	0.03	0.0591	0.0016	0.457	0.069	0.0561	0.0082	370	10	382	50	456	362
14.1	31	11	0.37	2	0.06	0.0583	0.0031	0.478	0.115	0.0595	0.0136	365	19	397	82	586	583
15.1	48	9	0.18	3	0.02	0.0573	0.0016	0.411	0.035	0.0521	0.0039	359	10	350	25	288	183
16.1	420	415	0.99	26	0.00	0.0537	0.0019	0.391	0.046	0.0528	0.0056	337	12	335	34	321	262
QES01 Andesite																	
1.1	95	58	0.61	5	0.01	0.0514	0.0012	0.371	0.035	0.0524	0.0046	323	7	321	26	301	214
2.1	63	28	0.45	3	0.03	0.0529	0.0015	0.412	0.043	0.0565	0.0054	332	9	350	31	472	228
3.1	78	39	0.50	4	0.02	0.0513	0.0017	0.373	0.044	0.0527	0.0057	323	10	322	33	315	268
4.1	67	33	0.49	3	0.06	0.0485	0.0017	0.354	0.110	0.0529	0.0162	305	10	308	86	325	900
5.1	84	44	0.52	4	0.03	0.0502	0.0016	0.345	0.052	0.0499	0.0071	315	10	301	40	189	301
6.1	79	42	0.53	5	0.03	0.0547	0.0012	0.403	0.044	0.0533	0.0056	344	7	343	32	343	255
7.1	79	39	0.49	4	0.05	0.0512	0.0017	0.350	0.106	0.0497	0.0148	322	10	305	83	178	897
8.1	81	46	0.57	4	0.05	0.0503	0.0026	0.360	0.056	0.0519	0.0073	317	16	312	43	281	292
9.1	84	45	0.54	5	0.02	0.0520	0.0015	0.391	0.033	0.0545	0.0041	327	9	335	24	391	176
10.1	88	42	0.48	5	0.05	0.0510	0.0023	0.361	0.085	0.0514	0.0116	321	14	313	66	257	451
11.1	118	64	0.55	6	0.03	0.0517	0.0015	0.369	0.049	0.0517	0.0065	325	9	319	37	273	272
12.1	90	45	0.50	5	0.03	0.0539	0.0015	0.412	0.038	0.0554	0.0047	339	9	350	28	427	199
QES02 Basaltic andesite																	
1.1	34	35	1.03	2	0.10	0.0476	0.0027	0.338	0.153	0.0514	0.0228	300	17	295	123	259	1562
2.1	251	233	0.93	13	0.01	0.0464	0.0008	0.341	0.028	0.0532	0.0042	292	5	298	21	339	187
3.1	34	20	0.60	2	0.09	0.0466	0.0022	0.396	0.131	0.0616	0.0198	294	14	339	100	661	661
4.1	65	45	0.70	4	0.04	0.0550	0.0024	0.387	0.111	0.0509	0.0142	345	15	332	85	238	812

Table 2 continued

Spot	U (ppm)	Th (ppm)	Th/U	Pb* (ppm)	$^{206}Pb_c$ (%)	$^{206}Pb^*/^{238}U$	error 1 σ	$^{207}Pb^*/^{235}U$	error 1 σ	$^{207}Pb^*/^{206}Pb^*$	error 1 σ	Age (Ma) $^{206}Pb^*/^{238}U$	error 1 σ	Age (Ma) $^{207}Pb^*/^{235}U$	error 1 σ	Age (Ma) $^{207}Pb^*/^{206}Pb^*$	error 1 σ
5.1	62	42	0.68	23	−0.01	0.3329	0.0096	5.330	0.274	0.1161	0.0045	1852	46	1874	45	1898	72
6.1	217	129	0.59	11	0.02	0.0497	0.0008	0.335	0.034	0.0488	0.0048	313	5	293	26	139	214
7.1	58	62	1.05	3	0.05	0.0470	0.0019	0.381	0.073	0.0589	0.0107	296	12	328	55	562	455
8.1	256	162	0.63	15	0.01	0.0554	0.0012	0.395	0.029	0.0518	0.0036	348	7	338	22	275	165
9.1	68	33	0.48	3	0.05	0.0486	0.0030	0.387	0.059	0.0577	0.0077	306	18	332	44	519	323
10.1	224	118	0.53	11	0.02	0.0483	0.0016	0.292	0.024	0.0439	0.0031	304	10	260	19	–	–
11.1	247	118	0.48	13	0.01	0.0496	0.0008	0.370	0.027	0.0541	0.0038	312	5	320	20	376	165
12.1	135	111	0.82	7	0.03	0.0487	0.0019	0.369	0.056	0.0550	0.0078	306	11	319	42	413	354
13.1	221	95	0.43	11	0.01	0.0490	0.0013	0.367	0.028	0.0543	0.0036	308	8	317	21	385	158
14.1	197	127	0.65	16	0.01	0.0732	0.0013	0.541	0.034	0.0536	0.0031	456	8	439	23	354	138
15.1	107	47	0.44	5	0.04	0.0480	0.0012	0.301	0.055	0.0455	0.0080	302	8	267	44	–	–
16.1	274	247	0.90	17	0.02	0.0529	0.0013	0.371	0.053	0.0509	0.0070	332	8	320	40	235	288
17.1	103	72	0.70	5	0.04	0.0464	0.0013	0.358	0.078	0.0561	0.0119	292	8	311	60	455	454
18.1	183	136	0.74	10	0.02	0.0490	0.0008	0.352	0.047	0.0521	0.0067	308	5	306	36	289	289

Pb_c indicates common Pb; Pb* indicates radiogenic Pb; Errors are 1σ

Table 3 Nd–Sr whole-rock isotopic data

Locality	Unit	Sample no.	Lithology	Age Ma	Rb ppm	Sr	Nd	Sm	$^{147}Sm/^{144}Nd$	$^{87}Rb/^{86}Sr$	$^{143}Nd/^{144}Nd$	$^{87}Sr/^{86}Sr$	Initial $^{87}Sr/^{86}Sr$	$\varepsilon_{Nd(t)}$
Quershan	Volcanic arc	QES01	Andesite	322 ± 3 Ma	3.91	476	14.52	3.33	0.1389	0.2375	0.512905 ± 0.000008	0.705000 ± 0.000014	0.7039	+7.6
		QES02	Basaltic andesite	304 ± 2 Ma	37.3	369	13.73	3.46	0.1526	0.2919	0.512858 ± 0.000006	0.704743 ± 0.000013	0.7035	+6.0
Hongshishan	Volcanic arc	HSS01	Basaltic andesite	Assumed at 357 Ma	1.92	225	10.50	2.73	0.1573	0.2467	0.512922 ± 0.000005	0.705245 ± 0.000010	0.7040	+7.3
		HSS02	Basalt		1.23	115	8.48	3.06	0.2184	0.0310	0.513202 ± 0.000014	0.704408 ± 0.000015	0.7043	+10.0
		HSS03	Basalt		0.333	746	2.96	1.50	0.3060	0.0129	0.513434 ± 0.000007	0.704010 ± 0.000014	0.7039	+10.6
		HSS04	Basalt		0.636	55.8	2.31	1.28	0.3334	0.0330	0.513512 ± 0.000005	0.705668 ± 0.000012	0.7055	+10.8
	Zoned mafic–ultramafic complex	HSS05-1	Gabbro	357 ± 4 Ma	0.452	49.9	1.25	0.61	0.2934	0.0262	0.513354 ± 0.000011	0.703225 ± 0.000014	0.7031	+9.6
		HSS05-2	leucogabbro	Assumed at 357 Ma	10.2	65.1	0.42	0.11	0.1614	0.4507	0.513079 ± 0.000010	0.704564 ± 0.000015	0.7023	+10.2
		HSS06	Harzburgite		0.443	10.2	0.23	0.08	0.2030	0.1258	0.513090 ± 0.000014	0.708153 ± 0.000015	0.7075	+8.5
		HSS07	Lherzolite		0.27	36.1	0.12	0.04	0.1879	0.0217	0.513061 ± 0.000016	0.704796 ± 0.000014	0.7047	+8.7

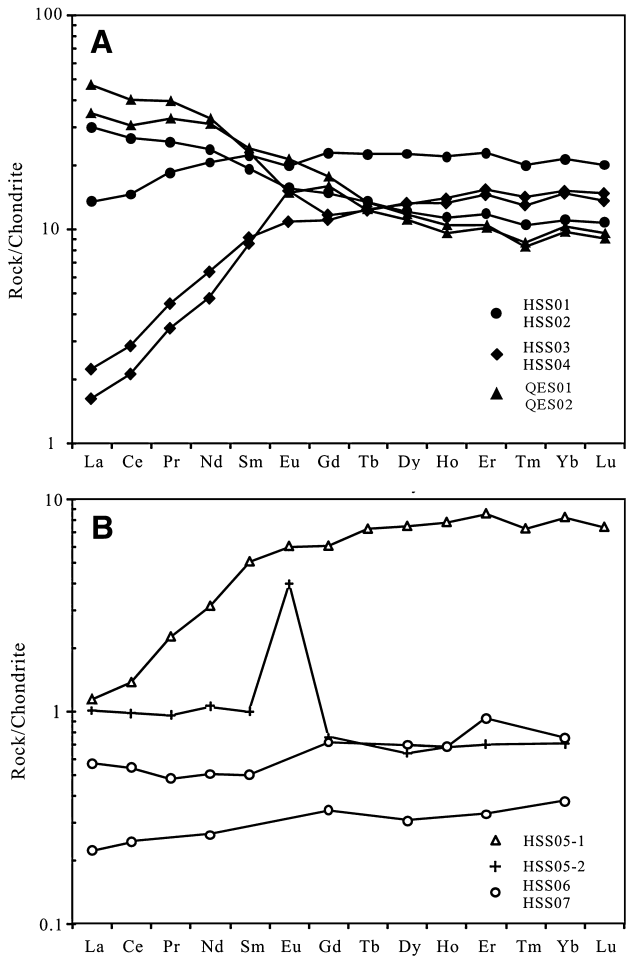

Fig. 3 Chondrite (CHON)-normalized REE patterns for samples of this study. Chondrite values are from Boynton (1984)

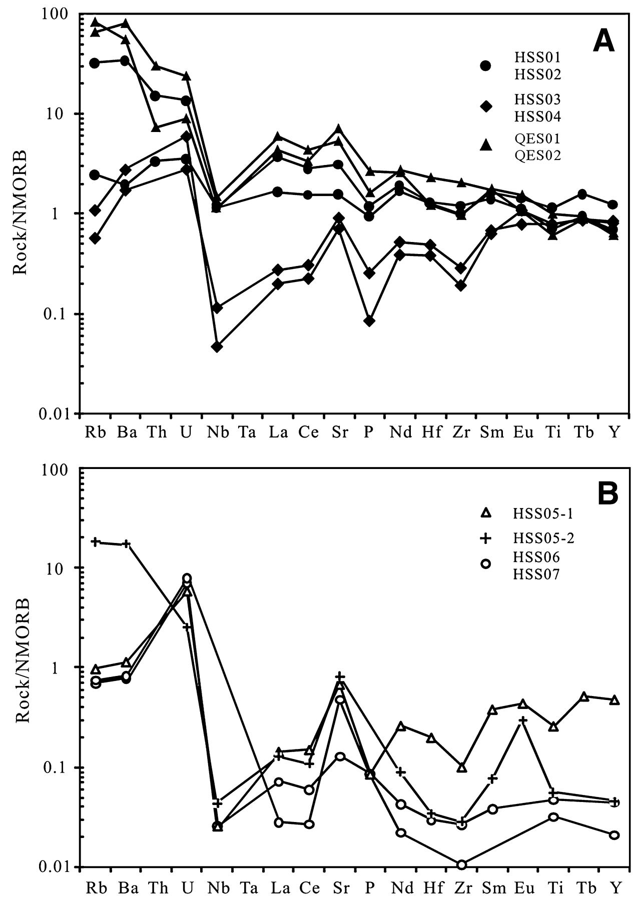

Fig. 4 N-MORB-normalized trace element variation diagrams for samples of this study. N-MORB values are from Sun and McDonough (1989)

time of andesite emplacement. Spots 6.1 (344 Ma) and 12.1 (339 Ma) are slightly older than the other spots and are understood to contain inherited Carboniferous grain components.

Most zircons from basaltic andesite sample QES02 are euhedral, and their CL images show broad and rhythmically zoned patterns (Fig. 6C), indicating a magmatic origin. Some zircons show core-rim structures suggesting some inheritance. Fourteen grain analyses from the basaltic andesite yielded concordant and near-concordant isotopic compositions with a weighted mean $^{206}Pb/^{238}U$ age of 304 ± 2 Ma ($\chi^2 = 1.51$) (Table 2; Fig. 7C) that we have interpreted to represent the time of basaltic andesite emplacement. Spots 4.1, 5.1, 8.1, 14.1, and 16.1 are older than the other spot analyses, and we interpret these as reflecting various degrees of inheritance.

4.3 Whole-rock Sr–Nd isotopic compositions

The harzburgite sample [$\varepsilon_{Nd(t)} = +8.5$, $I_{Sr} = 0.7075$] shows high I_{Sr} but a similar initial Nd isotope composition as the lherzolite sample [$\varepsilon_{Nd(t)} = +8.7$, $I_{Sr} = 0.7047$] (Table 3; Fig. 8), We have interpreted this I_{Sr} as disturbed, probably due to serpentinization or sub-ocean alteration.

Hongshishan gabbro [$\varepsilon_{Nd(t)} = +9.6 - +10.2$] and basalt [$\varepsilon_{Nd(t)} = +10.0 - +10.8$] samples show higher $\varepsilon_{Nd(t)}$ values than those of the ultramafic rocks, and they are also higher than that of Permo-Carboniferous NMORB (Table 3; Fig. 8), which suggests that these rocks are derived from a more depleted source than NMORB.

Quershan andesite [$\varepsilon_{Nd(t)} = +7.6$, $I_{Sr} = 0.7039$] and basaltic andesite [$\varepsilon_{Nd(t)} = +6.0$, $I_{Sr} = 0.7035$] have similar Nd–Sr isotopic compositions as the Hongshishan basaltic andesite [$\varepsilon_{Nd(t)} = +7.3$, $I_{Sr} = 0.7040$], and all these belong to arc tholeiites (Table 3; Fig. 8).

5 Discussion

5.1 Petrogenesis

Ophiolites represent remnants of oceanic lithosphere preserved in orogenic belts and mark suture zones between

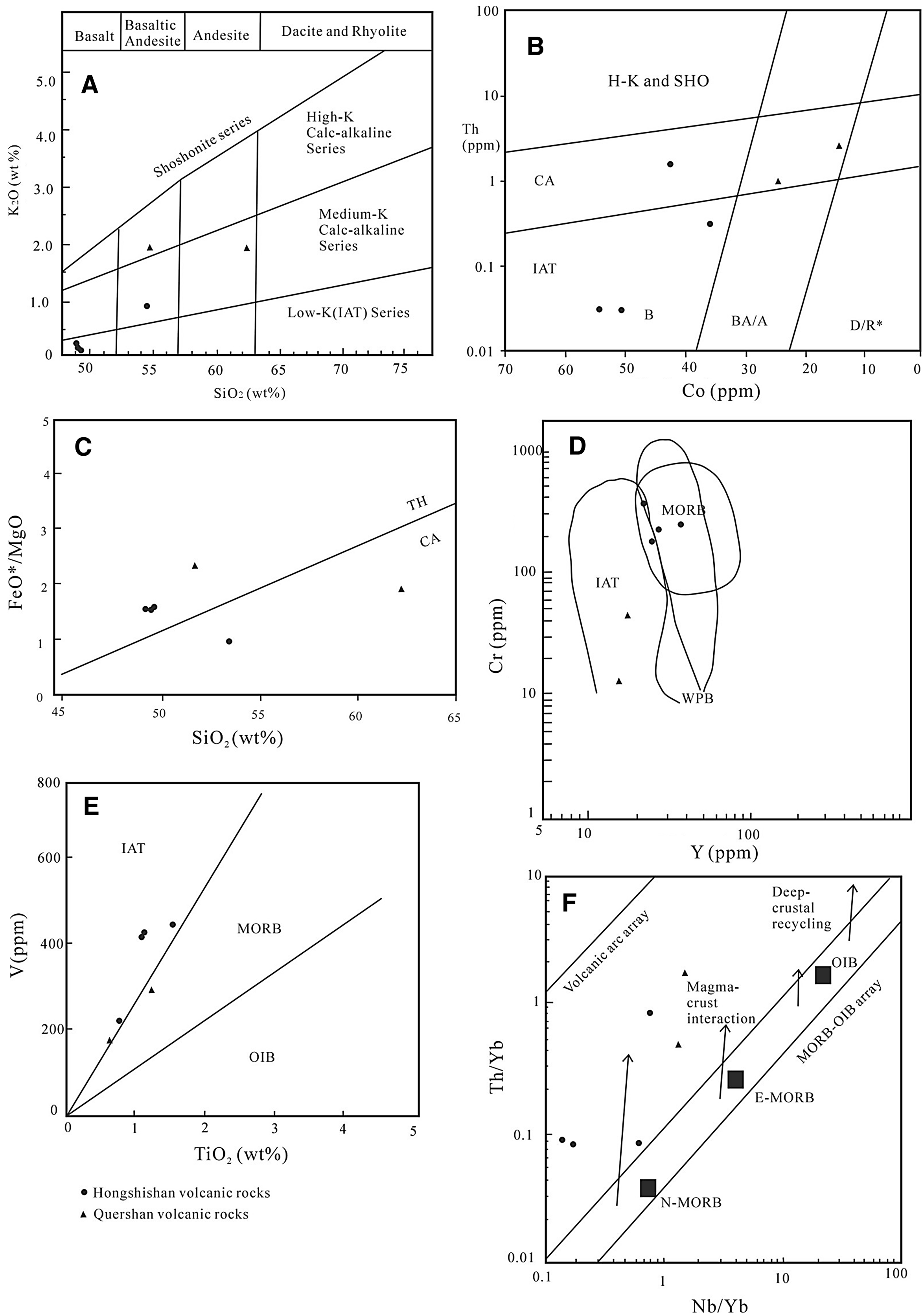

Fig. 5 The diagrams of K_2O–SiO_2 (**A** Le Maitre et al. 1989), Th–Co (**B** Hastie et al. 2007), FeO*/MgO–SiO_2 (**C** Miyashiro 1974), Cr–Y (**D** Pearce 1982), V–TiO_2 (**E** Shervais 1982), and Th/Yb–Nb/Yb (**F** Pearce 2008) for samples in this study

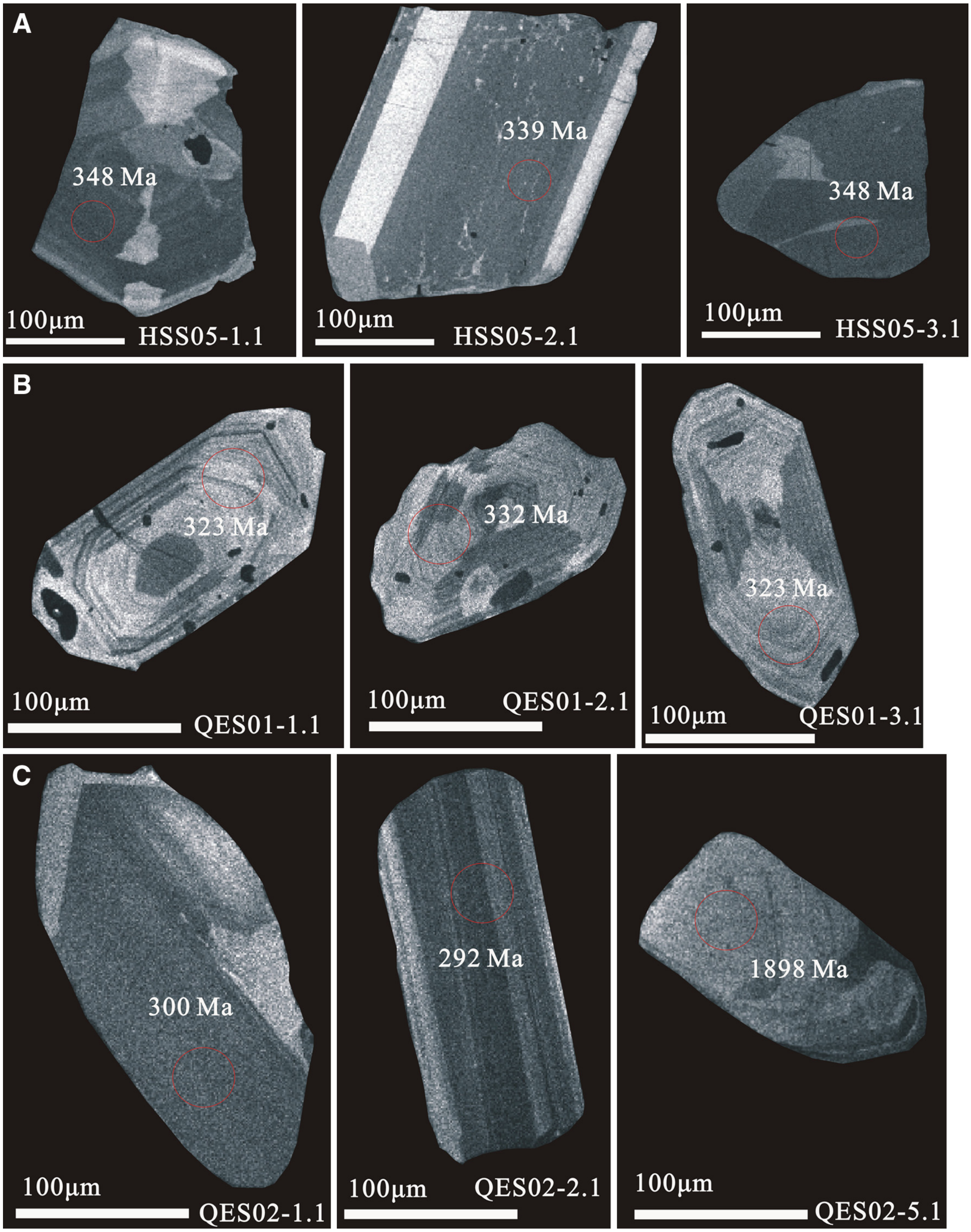

Fig. 6 Cathodoluminescence (CL) images and SHRIMP U–Pb ages of representative zircons from samples of this study

crustal blocks. They include, from bottom to top, ultramafic rocks (harzburgite, wherlite, dunite), layered and isotropic gabbro, sheeted dikes, basalt and a pelagic-hemipelagic sedimentary cover (Penrose Conference 1972). Ophiolitic fragments are widely distributed in the Beishan area (Zuo et al. 1987, 2003), northwestern China, which is located at the southern margin of the Central Asian Orogenic Belt (Fig. 1B).

However, Alaskan-type complexes are markedly concentrically zoned and generally composed of dunite, wehrlite, olivine clinopyroxenite, clinopyroxenite, hornblende clinopyroxenite, and gabbro. These complexes were

Fig. 7 Concordia diagrams for zircon analyses of samples

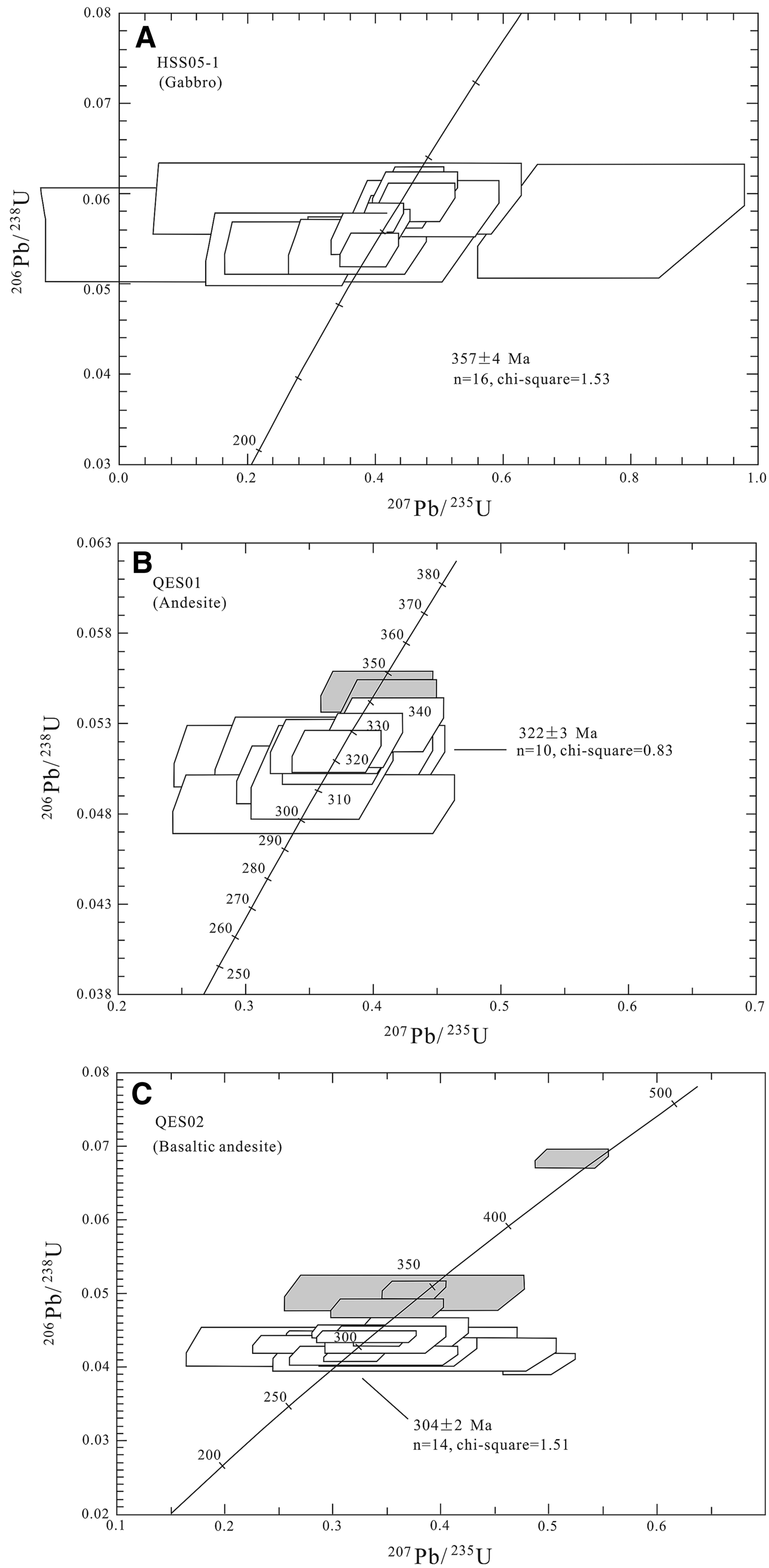

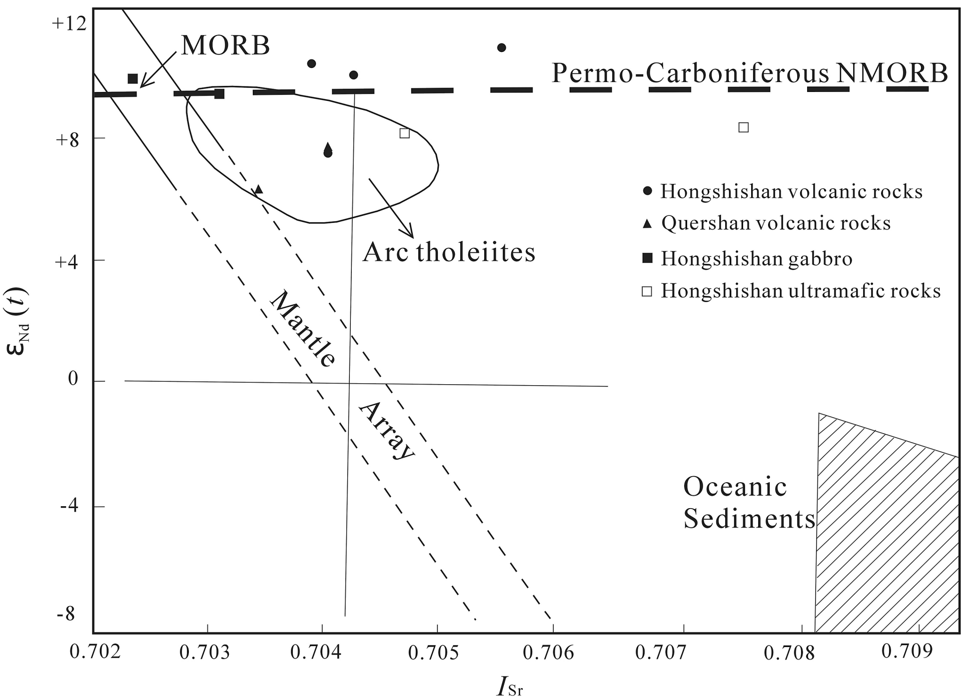

Fig. 8 I_{Sr} versus $\varepsilon_{Nd(t)}$ for samples in this study

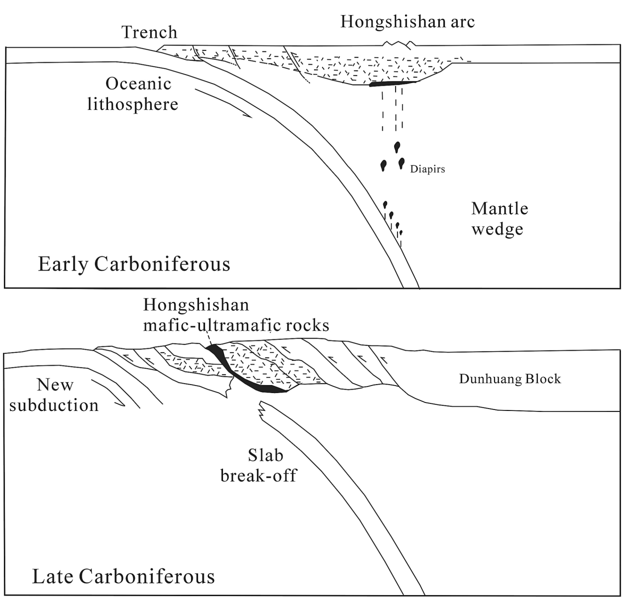

Fig. 9 A possible model to show the evolution of Beishan area, southern margin of CAOB during the Carboniferous (after DeBari and Coleman 1989)

believed to result from fractional melting in the mantle (Taylor 1967). Some ultramafic rocks have cumulus textures that reflect their origin and concentration through crystal fractionation processes (Murray 1972; Himmelberg and Loney 1994). Sha (1995) suggested that Alaskan-type complexes are fractionally derived from a mixture between a mantle-derived mafic magma and a crustal felsic magma. In contrast, Farahat and Helmy (2006) thought that there was no significant crustal contamination during the formation of Alaskan-type complexes through fractional crystallization of a hydrous parental magma.

Higher $\varepsilon_{Nd(t)}$ values than that of Permo-Carboniferous NMORB (Nelson and DePaolo 1984) (Table 3; Fig. 8) suggest that the Hongshishan gabbro and basalt were derived from a more depleted source than NMORB. The lower $\varepsilon_{Nd(t)}$ values of the ultramafic rocks may indicate later reaction of the parental magma with continental crust. We therefore suggest that the Hongshishan mafic–ultramafic complex is derived from a depleted mantle and that the ultramafic rocks experienced sub-ocean alteration.

5.2 Comparisons to regional mafic–ultramafic rocks

Three phases of mafic–ultramafic rocks occur in the Beishan area along the Sino–Mongolian boundary (Fig. 1B). Permian mafic–ultramafic complexes are found in the Eastern Tianshan and Beishan areas and in the Xinjing Uygur Autonomous Region (Zhou et al. 2004; Chai et al. 2008; Ao et al. 2010; Qin et al. 2011; Su et al. 2011, 2012; Song et al. 2013; Xue et al. 2016). Their rock types are mainly dunite, clinopyroxene peridotite, clinopyroxenite, gabbro, and diorite. These complexes have been interpreted as evolving from high-Mg tholeiitic magmas from the lithospheric mantle in a post-orogenic extensional tectonic setting and/or related to a mantle plume (Zhou et al. 2004; Han et al. 2006; Jiang et al. 2006; Wang et al. 2006; Chai et al. 2008; Zhang et al. 2008; Su et al. 2012; Qin et al. 2011), or related to asthenosphere upwelling (Song et al. 2013; Xue et al. 2016).

Cambrian mafic–ultramafic rocks of ophiolitic affinity consist of dunite, harzburgite, gabbro, diabase, and basalt (Shi et al. 2017), whose chemistry suggests a typical arc-trench complex. In this, a supra-subduction zone ophiolite records successive phases during its life cycle: birth (ca. 535 Ma), when the ocean floor of the ophiolite was formed; youth (ca. 533 Ma), characterized by mantle wedge magmatism; maturity (527–521 Ma), when basalt, basaltic andesite, andesite, and dacite were produced by slab melting and subsequent interaction of the melt with the mantle wedge; death (<519 Ma), caused by break-off of subducted slab and exhumation of the arc island.

The Carboniferous Alaskan-type complex is distinctly different in emplacement age and petrology from other regional mafic–ultramafic rocks, indicating that its petrogenesis and tectonic environment are different from that of the other two types.

5.3 Tectonic implications

Alaskan-type complexes have always been related to the subduction environment. Most researchers suggest that these complexes formed at convergent plate margins, representing arc magmas (Taylor 1967; Irvine 1974) or arc-root complexes (DeBari and Coleman 1989; Brugmann et al. 1997).

The Hongshishan complex is interpreted to constitute the remains of a magma chamber that crystallized at the base of a mature island arc (Fig. 9). The Late Carboniferous Quershan island arc volcanic rocks suggest resurrection of the subduction process after the collision of the Hongshishan arc and the Dunhuang Block, and then after uplift of the roots of the Early Carboniferous island arc (Fig. 9).

The Central Asian Orogenic Belt (CAOB) is a giant accretionary orogen revealing a complex evolution involving several subduction systems with different polarities and collision/accretion of arcs and microcontinents (Coleman 1989; Mossakovskii et al. 1993; Kröner et al. 2007, 2014; Windley et al. 2007; Jian et al. 2008, 2010a, b, 2014; Shi et al. 2016). Our identification of the early Carboniferous Hongshishan Alaskan-type complex and the Late Carboniferous Quershan island arc volcanic rocks along the southern margin of CAOB provides the necessary evidence to reconstruct a Late Paleozoic subduction process along the southern margin of the CAOB following early Paleozoic subduction (Shi et al. 2016).

6 Conclusions

1. The Hongshishan mafic–ultramafic complex mainly consists of dunite, harzburgite, lherzolite, wehrlite, and gabbro, and displays a zoned structure.
2. High $\varepsilon_{Nd(t)}$ values for the Hongshishan gabbro [$\varepsilon_{Nd(t)} = +9.6 - +10.2$] and basalt [$\varepsilon_{Nd(t)} = +10.0 - +10.8$] suggest that it is derived from a depleted mantle source. In contrast, the Late Carboniferous Quershan volcanic rocks are subduction-related arc rocks with Adakite-like compositions.
3. The Hongshishan complex represents the remains of a magma chamber that crystallized at the base of a mature island arc. The Late Carboniferous Quershan island arc volcanic rocks suggest resurrection of the subduction process after arc-continent collision and uplift of the roots of the Early Carboniferous island arc.

Acknowledgements We appreciate the editorial patience of Binbin Wang and Congqiang Liu. The comments of the anonymous reviewers are gratefully acknowledged. This study was financially supported by the National Natural Science Foundation of China (Grant Nos. 40703012, 41030314), Geological Survey of China (Grant Nos. 1212011120332, DD20160123-05), and Chinese Ministry of Science and Technology (Grant 2012FY120100).

References

Ao SJ, Xiao WJ, Han CM, Mao QG, Zhang JE (2010) Geochronology and geochemistry of Early Permian mafic–ultramafic complexes in the Beishan area, Xinjiang, NW China: implications for Late Paleozoic tectonic evolution of the southern Altaids. Gondwana Res 18:466–478

Ao SJ, Xiao WJ, Han CM, Li XH, Qu JF, Zhang JE, Guo QQ, Tian ZH (2012) Cambrian to Early Silurian ophiolite and accretionary processes in the Beishan collage, NW China: implications for the architecture of the Southern Altaids. Geol Mag 149:606–625

Badarch G, Cunningham WD, Windley BF (2002) A new terrane subdivision for Mongolia: implications for the Phanerozoic crustal growth of Central Asia. J Asian Earth Sci 21(1):87–110

Black LP, Jagodzinski EA (2003) Importance of establishing sources of uncertainty for the derivation of reliable SHRIMP ages. Aust J Earth Sci 50:503–512

Black LP, Kamo SL, Allen CM, Aleinikoff JN, Davis DW, Korsch RJ, Foudoulis C (2003) TEMORA 1: a new zircon standard for Phanerozoic U–Pb geochronology. Chem Geol 200:155–170

Boynton WV (1984) Cosmochemistry of the rare earth elements: meteorite studies. In: Henderson P (ed) Rare earth element geochemistry. Elsevier, Amsterdam, pp 63–114

Brugmann GE, Reischmann T, Naldrett AJ, Sutcliffe RH (1997) Roots of an Archean volcanic arc complex: the Lac des Iles area in Ontario, Canada. Precambrian Res 81:223–239

Chai FM, Zhang ZC, Mao JW, Dong LH, Zhang ZH, Wu H (2008) Geology, petrology and geochemistry of the Baishiquan Ni–Cu-bearing mafic–ultramafic intrusions in Xinjiang, NW China: implications for tectonics and genesis of ores. J Asian Earth Sci 32:218–235

Coleman RG (1989) Continental growth of Northwest China. Tectonics 8:621–635

DeBari SM, Coleman RG (1989) Examination of the deep levels of an island arc: evidence from the Tonsina ultramafic-mafic assemblage, Tonsina, Alaska. J Geophys Res 94:4373–4391

Dobretsov NL, Berzin NA, Buslov MM (1995) Opening and tectonic evolution of the Paleo-Asian Ocean. Int Geol Rev 37(4):335–360

Farahat ES, Helmy HM (2006) Abu Hamamid Neoproterozoic Alaskan-type complex, south Eastern Desert, Egypt. J Afr Earth Sci 45:187–197

Fershtater GB, Montero P, Borodina NS, Pushkarev EV, Smirnov VN, Bea F (1997) Uralian magmatism: an overview. Tectonophysics 276:87–102

Gill JB (1981) Orogenic andesites and plate tectonics. Springer, Berlin

Han CM, Xiao WJ, Zhao GC, Mao JW, Li SZ, Yan Z, Mao QG (2006) Major types, characteristics and geodynamic mechanism of Upper Paleozoic copper deposits in northern Xinjiang, northwestern China. Ore Geol Rev 28:308–328

Hastie AR, Kerr AC, Pearce JA, Mitchell SF (2007) Classification of altered volcanic island arc rocks using immobile trace elements: development of the Th–Co discrimination diagram. J Petrol 48:2341–2357

Hawkins JW (2003) Geology of supra-subduction zones-implications for the origin of ophiolites. In: Dilek Y, Newcomb S (eds) Ophiolite concept and the evolution of geological thought, vol 373. Geological Society of America Special Paper, pp 227–268

Helmy HM, El Mahallawi MM (2003) Gabbro Akarem mafic–ultramafic complex, Eastern Desert, Egypt: a Late Precambrian analogue of Alaskan-type complexes. Miner Petrol 77:85–108

Himmelberg GR, Loney RA (1994) Characteristics and petrogenesis of Alaskan-type ultramafic-mafic intrusions, Southeastern Alaska. US Geological Survey, Professional papers 1564, U.S. Government Printing Office, Washington, DC, pp 1–47

Huang ZB, Jin X (2006) Tectonic environment of basic volcanic rocks in the Hongshishan ophiolite mélange zone, Beishan mountains, Gansu. Geol China 33:1030–1037 **(in Chinese with English abstract)**

Irvine TN (1974) Petrology of the Duke island ultramafic complex southeastern Alaska. Geol Soc Am Mem 138:1–244

Jahn BM, Wu FY, Chen B (2000) Granitoids of the Central Asian Orogenic Belt and continental growth in the Phanerozoic. Trans R Soc Edinb: Earth Sci 91:181–193

Jian P, Shi YR, Zhang FQ, Miao LC, Zhang LQ, Kröner A (2007) Geological excursion to Inner Mongolia, China, to study the accretionary evolution of the southern margin of the Central Asian Orogenic Belt. Structural and tectonic correlation across the Central Asia Orogenic Collage: implications for continental growth and intracontinental deformation (Abstracts and Excursion guidebook). In: The 3rd international workshop and field excursions for IGC Project 480, pp 49–72

Jian P, Liu DY, Kröner A, Windley BF, Shi YR, Zhang FQ, Shi GH, Miao LC, Zhang W, Zhang Q (2008) Time scale of an early to mid-Paleozoic orogenic cycle of the long-lived Central Asian Orogenic Belt, Inner Mongolia of China: implications for continental growth. Lithos 101:233–259

Jian P, Liu DY, Kröner A, Windley BF, Shi YR, Zhang W, Zhang FQ, Miao LC, Zhang LQ, Tomurhuu D (2010a) Evolution of a Permian intraoceanic arc–trench system in the Solonker suture zone, Central Asian Orogenic Belt, China and Mongolia. Lithos 118(1):169–190

Jian P, Kröner A, Windley BF, Shi YR, Zhang W, Zhang LQ, Yang WR (2010b) Carboniferous and Cretaceous mafic–ultramafic massifs in Inner Mongolia (China): a SHRIMP zircon and geochemical study of the previously presumed integral "Hegenshan ophiolite". Lithos 142–143:48–66

Jian P, Kröner A, Jahn BM, Windley BF, Shi YR, Zhang W, Zhang FQ, Miao LC, Tomurhuu D, Liu DY (2014) Zircon dating of Neoproterozoic and Cambrian ophiolites in West Mongolia and implications for the timing of orogenic processes in the central part of the Central Asian Orogenic Belt. Earth Sci Rev 133:62–93

Jiang CY, Cheng SL, Ye SF, Xia MZ, Jiang HB, Dai YC (2006) Lithogeochemistry and petrogenesis of Zhongposhanbei mafic rock body, at Beishan region, Xinjiang. Acta Petrolog Sin 22:115–126 **(in Chinese with English abstract)**

Kröner A, Windley BF, Badarch G, Tomurtogoo O, Hegner E, Jahn BM, Gruschka S, Khain EV, Demoux A, Wingate MTD (2007) Accretionary growth and crust formation in the Central Asian Orogenic Belt and comparison with the Arabian-Nubian-Shield. Geol Soc Am Mem 200:181–209

Kröner A, Kovach V, Belousova E, Hegner E, Armstrong R, Dolgopolova A, Seltmann R, Alexeiev DV, Hoffmann JE, Wong J, Sun M, Cai K, Wang T, Tong Y, Wilde SA, Degtyarev KE, Rytsk E (2014) Reassessment of continental growth during the accretionary history of the Central Asian Orogenic Belt. Gondwana Res 25:103–125

Le Maitre RW, Bateman P, Dudek A, Keller J, Lameyre Le Bas MJ, Sabine PA, Schmid R, Sorensen H, Streckeisen A, Woolley AR, Zanettin B (1989) A classification of igneous rocks and a glossary of terms. Recommendations of the IGUS sub-commission on the systematic of igneous rocks. Blackwell, Oxford

Miyashiro A (1974) Volcanic rock series in island arcs and active continental margins. Am J Sci 274:321–355

Mossakovskii AA, Ruzhentsev SV, Samygin SG, Kheraskova TN (1993) Central Asian Foldbelt: geodynamic evolution and formation history. Geotektonika 6:3–32 **(in Russian)**

Murray CG (1972) Zoned ultramafic complexes of the Alaskan type: feeder pipes of andesitic volcanoes. Geol Soc Am Mem 132:313–335

Nelson BK, DePaolo DJ (1984) Rapid production of continental crust 1.7 to 1.9 b.y. ago: Nd isotopic evidence from the basement of the North American mid-continent. Geol Soc Am Bull 96:746–754

Pearce JA (1982) Trace element characteristics of lava from destructive plate boundaries. In: Thorpe RS (ed) Andesites. Wiley, Chichester, pp 525–548

Pearce JA (2008) Geochemical fingerprinting of oceanic basalts with applications to ophiolite classification and the search for Archean oceanic crust. Lithos 100:14–48

Penrose Conference (1972) Penrose field conference on ophiolites. Geotimes 17:24–25

Qin KZ, Su BX, Sakyi PA, Tang DM, Li XH, Sun H, Xiao QH, Liu PP (2011) SIMS zircon U–Pb geochronology and Sr–Nd isotopes of Ni–Cu-bearing mafic–ultramafic intrusions in Eastern Tianshan and Beishan in correlation with flood basalts in Tarim basin (NW China): constraints on a ca. 280 Ma mantle plume. Am J Sci 311:237–260

Sha LK (1995) Genesis of zoned hydrous ultramafic/mafic-silicic intrusive complexes: an MHFC hypothesis. Earth Sci Rev 39:59–90

Shervais JW (1982) Ti-V plots and the petrogenesis of modern and ophiolitic lavas. Earth Planet Sci Lett 59:101–118

Shervais JW (2001) Birth, death, and resurrection: the life cycle of suprasubduction zone ophiolites. Geochem Geophys Geosyst. doi:10.1029/2000GC000080

Shi YR, Jian P, Kröner A, Li LL, Liu C, Zhang W (2016) Zircon ages and Hf isotopic compositions of Ordovician and Carboniferous granitoids from central Inner Mongolia and their significance for Early and Late Paleozoic evolution of the Central Asian Orogenic Belt. J Asian Earth Sci 117:153–169

Shi YR, Zhang W, Kröner A, Li LL, Jian P (2017) Cambrian ophiolite fragments along the China–Mongolian border, southern margin of the Central Asian Orogenic Belt (**in press**)

Song XY, Chen LM, Deng YF, Xie W (2013) Syncollisional tholeiitic magmatism induced by asthenosphere upwelling owing to slab detachment at the southern margin of the Central Asian Orogenic Belt. J Geol Soc 170:941–950

Su BX, Qin KZ, Sakyi PA, Li XH, Yang YH, Sun H, Tang DM, Liu PP, Xiao QH, Malaviarachchi SPK (2011) U–Pb ages and Hf–O isotopes of zircons from Late Paelozoic mafic–ultramafic units in the southern Central Asian Orogenic Belt: tectonic implications and evidence for an Early-Permian mantle plume. Gondwana Res 20:516–531

Su BX, Qin KZ, Sakyi PA, Tang DM, Liu PP, Malaviarachchi SPK, Xiao QH, Sun H (2012) Geochronologic-petrochemical studies of the Hongshishan mafic–ultramafic intrusion, Beishan area, Xinjiang (NW China): petrogenesis and tectonic implications. Int Geol Rev 54:270–289

Sun SS, McDonough WF (1989) Chemical and isotopic systematics of oceanic basalts: implications for mantle composition and processes. Geol Soc Lond Spec Publ 42:313–345

Tang KD (1990) Tectonic development of Paleozoic foldbelts at the north margin of the Sino–Korean craton. Tectonics 9:249–260

Taylor HP (1967) The zoned ultramafic complexes of southeastern Alaska. In: Wyllie PJ (ed) Ultramafic and related rocks. Wiley, New York, pp 97–121

Wang JB, Wang YW, He HJ (2006) Ore deposits as a guide to the tectonic evolution in the East Tianshan Mountains, NW China. Geol China 33:461–469 **(in Chinese with English abstract)**

Wang GQ, Li XM, Xu XY, Yu JY, Wu P (2014) Ziron U–Pb chronological study of the Hongshishan ophiolite in the Beishan area and their tectonic significance. Acta Petrolog Sin 30:1685–1694

Wei ZJ, Huang ZB, Jin X, Sun YJ, Huo JC (2004) Geological characteristics of ophiolite migmatitic complex of Hongshishan region, Gansu. Northwest Geol 37:13–18 **(in Chinese with English abstract)**

Williams IS (1998) U–Th–Pb geochronology by ion microprobe. Applications of microanalytical techniques to understanding mineralizing processes. In: McKibben MA, Shanks III WC, Ridley WI (eds) Reviews in economic geology, vol 7. Society of Economic Geologists, Littleton, pp 1–35

Windley BF, Alexeiev D, Xiao WJ, Kröner A, Badarch G (2007) Tectonic models for accretion of the Central Asian Orogenic Belt. J Geol Soc 164(1):31–47

Xiao WJ, Windley BF, Hao J, Zhai MG (2003) Accretion leading to collision and the Permian Solonker suture, Inner Mongolia, China: termination of the central Asian orogenic belt. Tectonics 22:8–20

Xiao WJ, Mao QG, Windley BF, Han CM, Qu JF, Zhang JE, Ao SJ, Guo QQ, Cleven NR, Lin SF, Shan YH, Li JL (2010) Paleozoic multiple accretionary and collisional processes of the Beishan orogenic collage. Am J Sci 310:1553–1594

Xue SC, Li CS, Qin KZ, Tang DM (2016) A non-plume model for the Permian protracted (266–286 Ma) basaltic magmatism in the Beishan-Tianshan region, Xinjiang, Western China. Lithos 256–257:243–249

Zhang YY, Guo ZJ (2008) Accurate constraint on formation and emplacement age of Hongliuhe ophiolite, boundary region between Xinjiang and Gansu Provinces and its tectonic implications. Acta Petrolog Sin 24:803–809 **(in Chinese with English abstract)**

Zhang ZQ, Liu DY, Fu GM (1994) Isotopic geochronology of metamorphic strata in North Qinling, China. Beijing: Geological Publishing House, p 191 (in Chinese)

Zhang LC, Qin KZ, Xiao WJ (2008) Multiple mineralization events in the eastern Tianshan district, NW China: isotopic geochronology and geological significance. J Asian Earth Sci 32:236–246

Zhou MF, Lesher CM, Yang ZX, Li JW, Sun M (2004) Geochemistry and petrogenesis of 270 Ma Ni–Cu-(PGE) sulfide-bearing mafic intrusions in the Huangshan district, Eastern Xinjiang, Northwest China: implications for the tectonic evolution of the Central Asian Orogenic Belt. Chem Geol 209:233–257

Zuo GC, Zhang SL, Xie W, Jin SQ (1987) Characteristics of the turbidite and volcanic sedimentary assemblages of Cambrian-Middle Ordovician in the Xichangjing area of Beishan. Acta Sedimentol Sin 5:63–71

Zuo GC, Liu YK, Liu CY (2003) Framework and evolution of the tectonic structure in Beishan area across Gansu Province, Xinjiang Autonomous Region and Inner Mongolia Autonomous Region. Acta Geol Gansu 12:1–15